HOKKAIDO UNIVERSITY

Title	Elementary steps at the surface of ice crystals visualized by advanced optical microscopy
Author(s)	Sazaki, Gen; Zepeda, Salvador; Nakatsubo, Shunichi et al.
Citation	Proceedings of the National Academy of Sciences of the United States of America, 107(46), 19702-19707 https://doi.org/10.1073/pnas.1008866107
Issue Date	2010-11-16
Doc URL	https://hdl.handle.net/2115/45419
Type	journal article
File Information	PNAS107-46_19702-19707.pdf

Hokkaido University Collection of Scholarly and Academic Papers : HUSCAP

Elementary steps at the surface of ice crystals visualized by advanced optical microscopy

Gen Sazaki[a,b,1], Salvador Zepeda[a], Shunichi Nakatsubo[a], Etsuro Yokoyama[c], Yoshinori Furukawa[a]

[a]Institute of Low Temperature Science, Hokkaido University, N19-W8, Kita-ku, Sapporo 011-0819, Japan

[b]Precursory Research for Embryonic Science and Technology (PRESTO), Japan Science and Technology Agency, 4-1-8 Honcho, Kawaguchi, Saitama 332-0012, Japan

[c]Computer Centre, Gakushuin University, 1-5-1 Mejiro, Toyoshima-ku, Tokyo 171-8588, Japan

Author contributions: G.S. and Y.F. designed research; G.S. and S.Z. performed research; S.N. produced the experimental system; E.Y. contributed image analysis; G.S. and Y.F. wrote the paper.

The authors declare no conflict of interest.

[1]To whom correspondence should be addressed. E-mail: sazaki@lowtem.hokudai.ac.jp.

(Phone: +81-11-706+6880, Fax: +81-11-706-6880)

This article contains supporting information online at www.pnas.org/cgi/content.full/

Classification: Major: Physical Science, Minor: Physics

Abstract

Due to the abundance of ice on earth, the phase transition of ice plays crucially important roles in various phenomena in nature. Hence, the molecular-level understanding of ice crystal surfaces holds the key to unlocking the secrets of a number of fields. In this study we demonstrate, by laser confocal microscopy combined with differential interference contrast microscopy, that elementary steps (the growing ends of ubiquitous molecular layers with the minimum height) of ice crystals and their dynamic behavior can be visualized directly at air-ice interfaces. We observed the appearance and lateral growth of two-dimensional (2D) islands on ice crystal surfaces. When the steps of neighboring 2D islands coalesced, the contrast of the steps always disappeared completely. We were able to discount the occurrence of steps too small to detect directly because we never observed the associated phenomena that would indicate their presence. In addition, classical 2D nucleation theory does not support the appearance of multi-layered 2D islands. Hence, we concluded that 2D islands with elementary height (0.37 and 0.39 nm on basal and prism faces, respectively) were visualized by our optical microscopy. On basal and prism faces, we also observed the spiral growth steps generated by screw dislocations. The distance between adjacent spiral steps on a prism face was about 1/20 of that on a basal face. Hence, the step ledge energy of a prism face was 1/20 of that on a basal face, in accord with the known lower-temperature roughening transition of the prism face.

\body

Introduction

Ice is one of the most abundant materials on earth, and its phase transition governs a wide variety of phenomena, such as weather, environment-related issues, life in a cryosphere, cosmic evolution, etc. Hence the molecular-level understanding of ice crystal surfaces is crucially important. For example, ice crystal surfaces play a key role in heterogeneous physical/chemical reactions, such as the degradation of ozone and organic compounds adsorbed on ice crystal surfaces by UV light irradiation (1-4), the suppression of the growth of ice in living things by antifreeze proteins adsorbed on ice crystal surfaces (5-8), etc., as well as in the growth and sublimation/melting of ice crystals.

A crystal bounded by flat crystal faces grows layer by layer (9, 10), utilizing laterally growing molecular layers that have the minimum height determined by the crystal structure. Hence, growing ends of such molecular layers, so-called “elementary steps”, which ubiquitously exist on a crystal surface, play a key role during the physical/chemical reactions and the growth and sublimation/melting of ice crystals. Therefore to clarify such phenomena at the molecular level, first one has to observe “elementary steps” on ice crystal surfaces.

Many optical microscopy studies have been carried out to date to observe the surface morphology of ice crystals, such as steps (11-15), height topography (16-23) and quasi-liquid layers (QLLs) (24, 25), by ordinary bright-field microscopy (11, 15, 16), differential interference contrast microscopy (12-14, 17, 21-23, 25), two-beam interferometry (18-20) and laser reflection microscopy (24). However, none of these studies could prove, by their optical observations, that they could visualize individual “elementary steps”, mainly due to the small reflectivity (1.8%) of air-ice interfaces. Although elementary steps of mineral crystals were visualized by traditional optical microscopy as early as the 1950s (26, 27), in such cases the coating of crystal surfaces with thin films of silver (nearly 100% reflectivity) was indispensable. However, after coating crystal surfaces, one cannot observe the dynamic behavior of elementary steps on such dead crystal surfaces. Hence, direct in-situ observation of elementary steps on “bare ice crystal surfaces” is still needed.

Atomic force microscopy (AFM) is the most popular technique used to observe solid surfaces at the molecular level. However, it is generally acknowledged that the molecular-level AFM observation of ice crystal surfaces is very difficult (28-33). Such

difficulty is partly due to QLLs, although the cause of this difficulty is not yet fully clarified. The presence of QLLs at air-ice interfaces prevents the precise scan of cantilevers in the lateral directions, because of strong surface tension existing between the cantilevers and QLLs. However, some studies have measured the thickness of QLLs by measuring force curves, scanning cantilevers in the vertical direction. To our knowledge, so far, only Zepeda and coworkers have succeeded in the AFM observation of "elementary steps" on ice crystal surfaces by covering the ice crystal surfaces with octane (a hydrophobic solvent) (33). Because of the difficulty in utilizing AFM at air-ice interfaces, we decided that advanced optical microscopy is probably a promising alternative to directly observe elementary steps on ice crystal surfaces.

From among the various kinds of advanced optical microscopy, we chose laser confocal microscopy combined with differential interference contrast microscopy (LCM-DIM). We have previously directly visualized elementary steps of protein crystals (>several nm in height) in aqueous protein solutions (~1% reflectivity) with a sufficient contrast level by this technique (34-37). Using LCM-DIM, we could also visualize dislocations in protein crystals during growth (38). Since LCM-DIM has a high detection sensitivity and is not affected by the observation environment, we were able to visualize elementary steps of protein crystals even in a gel (39) and under high pressure (40). Such high detection sensitivity coupled with an insensitivity to the environment makes this technique look very promising, in particular for observing air-ice interfaces at a temperature just below the melting point of ice. In this study, we further improved the detection sensitivity of LCM-DIM, and attempted the visualization of elementary steps at air-ice interfaces.

Results and Discussion

Basal faces grown by two-dimensional nucleation and subsequent lateral growth. We grew Ih ice single crystals heteroepitaxially on a cleaved {0001} face of an AgI crystal from supersaturated water vapor in a nitrogen environment. We set the temperature of the ice single crystals (T_{sample}) at -15.0°C, at which temperature basal ({0001}) faces of ice crystals develop most widely (41). To supply water vapor to the sample ice crystals, we prepared other ice crystals (as a source of water vapor) on a copper plate that was 16 mm distant from the AgI crystal, and then separately set the temperature of the source ice crystals (T_{source}) at -13.0°C. By changing T_{sample} and T_{source},

we adjusted the growth temperature of the sample ice crystals and the supersaturation of water vapor (the driving force for crystallization) separately. In our experiments, the exact evaluation of supersaturation was difficult, because of the uncertainty in the temperature of water vapor in the vicinity of the sample ice crystals. The details of all these operations are explained in the Materials and Methods section. Hence, hereafter, to notate the growth conditions, we list values of T_{sample} and T_{source}, rather than try to estimate the actual degree of supersaturation.

Fig. 1 shows typical examples of the surface morphology of the basal face of a sample ice crystal observed by our improved LCM-DIM, by which steps with subnanometer height on a transparent crystal surface could be visualized, as explained in the Materials and Methods section. T_{sample} and T_{source} were -10.0 and -9.3°C, respectively. Photomicrographs of 720×208 pixels were acquired over a 0.57 s scan time. To obtain the images shown in Fig. 1, raw images were processed according to the recipe explained in the supporting information (Fig. S1). We subtracted the time-averaged image (Fig. S1b), in which motionless objects such as defects (a white arrowhead in Fig. S1b) and the inhomogeneous background level were recorded, from the original image (Fig. S1a). After the adjustment of a gain and an offset (Fig. S1c), a Gaussian filter of one pixel size was used to smooth the image (Fig. S1d).

As shown in Figs. 1a–1d taken at 0.57 s intervals, the basal face of the ice crystal grew by a two-dimensional (2D) nucleation growth mode of birth-and-spread type. The 2D islands appeared and then spread laterally with growth time. The isotropic round shape of the 2D islands agrees with that observed for sublimation steps at temperatures above -20°C (15). When the steps of neighboring 2D islands coalesced, contrast of the steps always disappeared completely, as in the regions indicated by cross marks in Figs. 1b and 1d. Videos of the appearance and lateral growth of 2D islands are available in the supporting information (Videos S1 and S2), in which the image processing shown in Fig. S1 was not performed (Video S1: just the gain and offset of original images were adjusted) and was performed (Video S2), respectively.

From the time course of the surface morphology observed during 100 s, we determined the positions at which 2D islands were formed and coalesced, as shown in Fig. 2. Asterisk marks (Fig. 2a) indicate the positions where 2D islands were newly formed. In the central region of the basal face, 2D islands appeared at random locations, demonstrating that in these regions 2D islands were formed by 2D nucleation. In contrast, in the peripheral

region, the 2D islands did not appear, probably suggesting that strain energy induced by defects, which generally tend to remain in the central region of a crystal surface, promoted the 2D nucleation in the central region (42, 43).

In Fig. 2b, cross marks correspond to the positions where the step contrast disappeared completely after the coalescence of neighboring 2D islands during 100 s of observation. Due to the spatial randomness of the 2D nucleation, the disappearances of the step contrast also occurred at random locations on the crystal surface. Fig. 2b shows such a typical example observed during 100 s at T_{sample}= -10.0 and T_{source}= -9.3°C. We could commonly observe such disappearances of the step contrast on ice crystal surfaces grown under various T_{sample}, although at $\Delta T \equiv T_{source} - T_{sample} > 1.5$°C the disappearances of the step contrast became difficult to observe because of the high densities and high lateral growth rates of 2D islands. Noteworthy is that no step contrast remained after the coalescence of neighboring 2D islands, indicating that no bunched (multi-layered) step were being produced.

Verification of the visualization of elementary steps. As a first step, it is important to prove whether or not the steps we observed were elementary steps, those which have the minimum height determined by the crystal structure. To discuss this issue quantitatively, we assumed two cases. The first is in which all steps that existed on the ice crystal surface could be fully visualized. The second is where there were invisible steps on the ice crystal surface: i.e. LCM-DIM could not visualize steps whose heights were smaller than a critical value h_{crit}.

In the first case, the complete disappearance of the step contrast after the coalescences shown in Figs. 1 and 2 indicates that the height of the steps of the 2D islands observed was identical: i.e. such steps can be described as “elementary steps” with the minimum height.

In the second case, we have to take into account the coalescence of a detectable step (whose height $h \geq h_{\mathrm{crit}}$) and an undetectable step (whose height $h' < h_{\mathrm{crit}}$). When the height difference $\Delta h \equiv h - h'$ is less than h_{crit}, the detectable step apparently disappears after the coalescence. Such apparent disappearance of the step contrast becomes more frequent with increasing h, as explained quantitatively in our previous paper (40). However, we never found such apparent disappearance of the step contrast throughout all of the experiments. This result strongly supports our hypothesis that h_{crit} is smaller than the height of the smallest steps: i.e., LCM-DIM could visualize elementary steps on the ice

crystal surface.

In addition, the second case violates the tenets of classical 2D nucleation theory, whose validity has been widely confirmed by many experiments (9, 10, 37, 44, 45). The 2D nucleation rate $J^{2D}(i)$ of multi-layered islands, where i is the number of layers, can be expressed as follows (9, 10):

$$J^{2D}(i) = \varpi\Gamma C_1 \cdot \exp\left(-\frac{i \cdot \Delta G(1)}{k_B T}\right). \quad (1)$$

Here ϖ is the attachment frequency of a monomeric molecule to a critical nucleus, Γ the Zeldovich factor, C_1 the density of monomeric molecules on a crystal surface, $\Delta G(1)$ the activation free energy barrier of the 2D nucleation of single-layered (elementary) islands, k_B the Boltzmann constant, T the absolute temperature. Hence the ratio of $J^{2D}(i)$ to $J^{2D}(1)$ (the 2D nucleation rate of single-layer (elementary) islands) is given by

$$\frac{J^{2D}(i)}{J^{2D}(1)} = \left[\exp\left(-\frac{\Delta G(1)}{k_B T}\right)\right]^{(i-1)} = \left[\frac{C(1)^*}{C_1}\right]^{(i-1)} \approx 0, \quad (2)$$

where $C(1)^*$ is the density of single-layered critical nuclei on a crystal surface. Since $C(1)^*$ is astronomically smaller than C_1, $J^{2D}(i)$ is negligibly small compared to $J^{2D}(1)$. Hence, we can conclude that the 2D islands visualized by LCM-DIM were single (elementary) layers.

So far, there are many papers that observed steps on ice crystal surfaces (11-15). However, these studies observed spiral growth steps, and hence failed to prove the observation of elementary steps. In this study, we have clearly observed 2D nucleation growth and verified that we are visualizing elementary steps. The keys to this achievement are the improvement to LCM-DIM explained in the Materials and Methods section and the preparation of high quality ice crystals.

Height of elementary steps. A schematic cross section of an ice crystal (Fig. 3) indicates that a basal face has a bilayer structure (46). The distance between adjacent bilayers is 0.37 nm, which is a half of a unit cell height in the *c* direction. Because of the tetrahedral bonding of water molecules in an ice crystal, the density of intrabilayer hydrogen bonding is three times higher than that between bilayers, strongly suggesting that a bilayer structure forms a topmost layer of a basal face. Therefore one could expect that the height of elementary steps on a basal face is 0.37 nm.

To our knowledge, Zepeda and coworkers are the only workers so far who have visualized “elementary steps” on ice crystal surfaces covered with octane by AFM, and

reported that the measured height of elementary steps of basal faces was 0.29 nm (33). Taking into account the large error of AFM measurements in the height direction, this height coincides well with the interbilayer height of 0.37 nm. Hence, we concluded that LCM-DIM could successfully visualize elementary steps of 0.37 nm height at the interface between air and a basal face.

Two-dimensional nucleation growth on prism faces. In addition to the ice crystals grown heteroepitaxially on the cleaved AgI crystal, we also found that a small number of ice crystals had randomly nucleated and grown with their prism ($\{10\bar{1}0\}$) faces (by chance) placed perpendicular to the optical axis. This fortunate occurrence meant that such prism faces could be observed by LCM-DIM.

Fig. 4 shows the time-course of a prism face taken by LCM-DIM. Photomicrographs of 512×448 pixels were acquired over a 0.99 s scan time. T_{sample} and T_{source} were -2.2 and -2.2°C, respectively (the supersaturation was very small). The crystallographic orientation of the crystal was determined from an image taken by ordinary bright-field optical microscopy (e.g. Fig. 6d). As shown in Figs. 4a-4d, the prism face also grew by a 2D nucleation growth mode of birth-and-spread type. The 2D islands appeared randomly on the prism face and spread in the lateral direction with growth time. Then, after the coalescence of neighboring 2D islands, the contrast of the steps disappeared completely, as in the regions indicated by cross marks in Figs. 4b and 4d. Such disappearances of the step contrast were consistently observed all over the prism faces examined. Therefore, following the same line of argument used for the basal face, we also concluded that LCM-DIM could visualize elementary steps on the prism face.

The height of elementary steps on a prism face is expected to be 0.39 nm from their crystallographic structure (also consisting of a bilayer structure), although no AFM measurement has yet been reported.

Spiral growth. Besides 2D nucleation growth, another important and ubiquitous growth mechanism is spiral growth (9, 10). In-situ observations of elementary spiral steps on basal and prism faces provide intrinsic information on this growth mode on these faces. Fig. 5 presents a basal face (a) and a prism face (b) growing by the spiral growth mechanism induced by screw dislocations (indicated by white arrowheads). Although the steps shown in Fig. 5a do not look like spiral steps because of the low step density (large step separation), growth under higher supersaturation provided much higher step density (smaller step separation), as shown in Fig. S2 in the supporting information. Hence we

could be sure that these features were really spiral steps.

The two crystals shown in Figs. 5a and 5b were adjacently located on the same AgI crystal. Hence, we can assume that the supersaturations provided for both crystal surfaces were almost the same. Nevertheless, the distance between the adjacent spiral steps on the basal face ($l^{basal} \cong 100\,\mu m$) was much longer than that on the prism face ($l^{prism} \cong 5\,\mu m$). The distance between adjacent spiral steps l can be expressed as follows (9, 10):

$$l = 19\rho_c = 19\frac{s\kappa}{\Delta\mu}. \quad (3)$$

Here ρ_c is the radius of a critical 2D nuclei, s the area one molecule occupies inside a 2D nucleus, κ the free energy of a step ledge, $\Delta\mu$ the driving force for crystallization (supersaturation). Therefore, the ratio of interstep distances corresponds to the ratio of the step ledge energies:

$$\frac{l^{basal}}{l^{prism}} = \frac{\kappa^{basal}}{\kappa^{prism}} \cong 20. \quad (4)$$

Much smaller κ^{prism} than κ^{basal} qualitatively coincides with the fact that the prism face roughens more easily (at a lower temperature) than the basal face (47).

Longstanding questions that will be explored by LCM-DIM. In this study, we demonstrated that LCM-DIM can visualize elementary steps on ice crystal surfaces directly with sufficient contrast levels in real time. Hence, we believe that LCM-DIM can become a promising means in the near future to explore many longstanding questions regarding ice crystals, such as the role of ice crystal surfaces in the heterogeneous physical/chemical reactions, the formation mechanisms and growth kinetics of QLLs induced by surface melting, roughening transitions of steps and crystal surfaces, evaluation of the step ledge free energy from the measurement of 2D nucleation rates, etc., in addition to the growth kinetics of elementary steps.

Materials and Methods

Observation system. A confocal system (FV300 [discontinued], Olympus Optical Co. Ltd.) was attached to an inverted optical microscope (IX70 [discontinued], Olympus Optical Co. Ltd.), as shown in Fig. 6a. A super luminescent diode (Amonics Ltd., model ASLD68-050-B-FA: 680 nm), whose coherent length and full-width at half-maximum were about 10 μm and 23 nm, was used for LCM-DIM observation to avoid the appearance of interference fringes. LCM significantly reduces the noise originating from

outside of the focal depth. In addition, DIM changes the phase difference between the two light beams reflected at both sides of a step (upper and lower terraces) into an intensity difference. By combining these two effects, LCM-DIM exhibits a high sensitivity in *z*-direction (34). In this study, a polarizer made of aligned silver nanoparticles (colorPol VISIR CWO2, CODIXX AG Co. Ltd.) and a polarization beam splitter (BL9004, Olympus Optical Co. Ltd.) were newly adopted to increase the illumination intensity and hence to further improve the signal-noise ratio of LCM. Also an analyzer used in our previous system was removed, since the polarization beam splitter provides the same function. A new low magnification objective (UPlanFl 10X P, Olympus Optical Co. Ltd.) was also used to avoid deterioration of the degree of polarization and hence to improve the DIM contrast further. Other details were reported in our previous studies (34, 36).

To prove the efficiency of the improved LCM-DIM system, a cleaved surface of a transparent gypsum crystal was observed by both LCM-DIM and AFM (Fig. S3 in the supporting information). The comparison of the same field of view observed by both methods clearly shows that steps of 0.75 nm height on a cleaved gypsum crystal could be visualized with sufficient contrast level by LCM-DIM.

Fig. 6b presents a sectional view of the observation chamber. The chamber was made of a teflon plate sandwiched between two copper plates. The temperatures of the upper and lower Cu plates were separately controlled using four Peltier elements (an exploded diagram of the chamber is shown in Fig. S4). At the center of the lower side of the upper Cu plate, a cleaved AgI crystal, which is known as an ice nucleating agent, was attached using heat grease. AgI crystals were a kind gift provided by emeritus professor Gary Layton of Northern Arizona University.

Growth of seed ice crystals. Temperatures of the upper and lower Cu plates were set at T_{sample}=20.0 and T_{source}=-15.0°C, respectively. Then water vapor was supplied to the inside of the chamber by nitrogen gas bubbled through water (flow rate: 500 mL/min). After source ice crystals were grown on the lower Cu plate for 1 hour, two valves on the chamber were closed to stop the water-vapor supply and to keep the chamber airtight. Then the temperatures of the upper and lower Cu plates were set at T_{sample}=-15.0 and T_{source}=-13.0°C, respectively, for 2 hours to nucleate sample ice crystals on the cleaved AgI crystal. Most of the ice crystals that appeared on the AgI crystal had the same orientation (inset of Fig. 6b), indicating that they were grown hetero-epitaxially. Then at T_{sample}=-15.0 and T_{source}=-14.0°C, the sample ice crystals were grown overnight until their

lateral size and height reached several hundred μm.

Figs. 6c and 6d respectively show the images of basal and prism faces of ice crystals observed by ordinary bright-field optical microscopy. In the case of a basal face, two facets with a dihedral angle of 120° clearly indicate their crystallographic orientation (Fig. 6c). However, in the case of a prism face, the crystallographic orientation is determined utilizing other prism faces (marked by white arrowheads in Fig. 6d) that are connected to the targeted prism face. As the shape of ice crystals became rounded close to the melting point (as shown in Fig. 4), the crystallographic orientation was determined at -15°C, at which temperature well-faceted crystals were obtained.

In the observation chamber the sample ice crystals were 16 mm away from the source ice crystals. As water vapor diffused away from the source ice crystals in N_2 gas at atmospheric pressure, its temperature increased. Hence the temperature of water vapor in the vicinity of the sample ice crystals was unclear, and in our observations, the degree of supersaturation could not be quantified exactly. This is evidenced by the fact that even when T_{sample} was slightly higher than T_{source}, like the case shown in Fig. 5, the growth of elementary steps was observed.

ACKNOWLEDGMENTS

The authors thank Y. Saito and S. Kobayashi (Olympus Engineering Co., Ltd.) for their technical support for the improvement of LCM-DIM, Gary Layton (Northern Arizona University) for the provision of AgI crystals, and T. Sei (Aichi Gakuin University) and H. Nada (National Institute of Advanced Industrial Science and Technology) for valuable discussions. This work was supported by JST PRESTO program.

References

1. Peter T (1997) Microphysics and heterogeneous chemistry of polar stratospheric clouds. *Annual Review of Physical Chemistry* 48:785-822.
2. Tabazadeh A, Turco RP, Drdla K, Jacobson MZ, & Toon OB (1994) A study of type-I polar stratospheric cloud formation. *Geophysical Research Letters* 21(15):1619-1622.
3. Kroes GJ & Clary DC (1992) Sticking of HCl and ClOH to ice - a computational study. *Journal of Physical Chemistry* 96(17):7079-7088.
4. Koehler BG, Middlebrook AM, & Tolbert MA (1992) Characterization of model

polar stratospheric cloud films using fourier-transform infrared-spedtroscopy and temperature programmed desorption. *Journal of Geophysical Research-Atmospheres* 97(D8):8065-8074.

5. Scholander PF, Van Dam L, Kanwisher JW, Hammel HT, & Gordon MS (1957) Supercooling and osmoregulation in arctic fish. *J. Cell Comp. Physiol.* 49:5-24.
6. Yeh Y & Feeney RE (1996) Antifreeze proteins: structures and mechanisms of function. *Chemical Reviews* 96(2):601-617.
7. Graham LA, Liou YC, Walker VK, & Davies PL (1997) Hyperactive antifreeze protein from beetles. *Nature* 388(6644):727-728.
8. Kawahara H (2002) The structures and functions of ice crystal-controlling proteins from bacteria. (Translated from English) *J. Biosci. Bioeng.* 94(6):492-496 (in English).
9. Chernov AA (1984) *Modern crystallography III* (Springerr-Verlag, Berlin) pp 127-129.
10. Markov IV (1995) *Crystal growth for beginners* (World Scientific Publishing, Singapore) pp 192-197.
11. Furukawa Y, Yamamoto M, & Kuroda T (1987) Ellipsometric study of the transition layer on the surface of an ice crystal. *Journal of Crystal Growth* 82:665-677.
12. Gonda T & Sei T (1987) The growth-mechanism of ice crytals grown in air at a low-pressure and their habit change with temperature. *Journal De Physique* 48(C-1):355-359.
13. Sei T & Gonda T (1989) The growth mechanism and the habit change of ice crystals growing from the vapor-phase. *Journal of Crystal Growth* 94(3):697-707.
14. Gonda T, Kakiuchi H, & Moriya K (1990) In situ observation of internal structure in growing ice crystals by laser scattering tomography. *Journal of Crystal Growth* 102(1-2):167-174.
15. Furukawa Y & Kohata S (1993) Temperature dependence of the growth form of negative crystal in an ice single crystal and evaporation kinetics for its surfaces. *Journal of Crystal Growth* 129(3-4):571-581.
16. Raymond JA, Wilson P, & Devries AL (1989) Inhibition of growth of nonbasal planes in ice by fish antifreezes. *Proceedings of the National Academy of Sciences of the United States of America* 86(3):881-885.

17. Sei T & Gonda T (1989) Growth rate of polyhedral ice crystals growing from the vapor-phase and their habit change. *Journal of the Meteorological Society of Japan* 67(4):495-502.
18. Furukawa Y & Shimada W (1993) Three-dimensional pattern formation during growth of ice dendrites -- its relation to universal law of dendritic growth. *Journal of Crystal Growth* 128(1-4):234.
19. Gonda T, Matsuura Y, & Sei T (1994) In situ observation of vapor-grown ice crystals by laser two-beam interferometry. *Journal of Crystal Growth* 142(1-2):171-176.
20. Shimada W & Furukawa Y (1997) Pattern formation of ice crystals during free growth in supercooled water. *Journal of Physical Chemistry B* 101(32):6171-6173.
21. Sei T, Gonda T, & Arima Y (2002) Growth rate and morphology of ice crystals growing in a solution of trehalose and water. *Journal of Crystal Growth* 240(1-2):218-229.
22. Gonda T & Sei T (2005) The inhibitory growth mechanism of saccharides on the growth of ice crystals from aqueous solutions. *Progress in Crystal Growth and Characterization of Materials* 51(1-3):70-80.
23. Sei T & Gonda T (2006) Melting point of ice in aqueous saccharide solutions. *Journal of Crystal Growth* 293(1):110-112.
24. Elbaum M, Lipson SG, & Dash JG (1993) Optical study of surface melting on ice. *Journal of Crystal Growth* 129(3-4):491-505.
25. Gonda T, Arai T, & Sei T (1999) Experimental study on the melting process of ice crystals just below the melting point. *Polar Meteorol. Glaciol.* 13:38-42.
26. Amelinckx S (1951) Spiral growth on carborundum crystal faces. *Nature* 167:939-940.
27. Griffin LJ (1950) Observation of unimolecular growth steps on crystal surfaces. *Pholosofical Magazine Series 7* 41:196-199.
28. Petrenko VF (1997) Study of the surface of ice, ice/solid and ice/liquid interfaces with scanning force microscopy. *Journal of Physical Chemistry B* 101(32):6276-6281.
29. Doppenschmidt A, Kappl M, & Butt HJ (1998) Surface properties of ice studied by atomic force microscopy. *Journal of Physical Chemistry B*

102(40):7813-7819.

30. Pittenger B, Cook DJ, Slaughterbeck CR, & Fain SC (1998) Investigation of ice-solid interfaces by force microscopy: Plastic flow and adhesive forces. *Journal of Vacuum Science & Technology a-Vacuum Surfaces and Films* 16(3):1832-1837.
31. Bluhm H & Salmeron M (1999) Growth of nanometer thin ice films from water vapor studied using scanning polarization force microscopy. *Journal of Chemical Physics* 111(15):6947-6954.
32. Ogawa K & Majumdar A (1999) Molecular-level imaging of ice crystal structure and dynamics by atomic force microscopy. *Microscale Thermophysical Engineering* 3(2):101-110.
33. Zepeda S (2004) Intermolecular interactions: from the hydrogen bond to biological function. Ph.D. (University of California, Davis).
34. Sazaki G, *et al.* (2004) In situ observation of elementary growth steps on the surface of protein crystals by laser confocal microscopy. *Journal of Crystal Growth* 262(1-4):536-542.
35. Van Driessche AES, *et al.* (2008) Comparison of Different Experimental Techniques for the Measurement of Crystal Growth Kinetics. *Crystal Growth & Design* 8(12):4316-4323.
36. Van Driessche AES, *et al.* (2009) Direct Observation of Adsorption Sites of Protein Impurities and Their Effects on Step Advancement of Protein Crystals. *Crystal Growth & Design* 9(7):3062-3071.
37. Van Driessche AES, *et al.* (2007) Direct and noninvasive observation of two-dimensional nucleation behavior of protein crystals by advanced optical microscopy. *Crystal Growth & Design* 7(10):1980-1987.
38. Sazaki G, Tsukamoto K, Yai S, Okada M, & Nakajima K (2005) In situ observation of dislocations in protein crystals during growth by advanced optical microscopy. *Crystal Growth & Design* 5(5):1729-1735.
39. Van Driessche AES, Otalora F, Gavira JA, & Sazaki G (2008) Is agarose an impurity or an impurity filter? In situ observation of the joint gel/impurity effect on protein crystal growth kinetics. *Crystal Growth & Design* 8(10):3623-3629.
40. Suzuki Y, *et al.* (2009) First Direct Observation of Elementary Steps on the Surfaces of Glucose Isomerase Crystals under High Pressure. *Crystal Growth &*

Design 9(10):4289-4295.

41. Nakaya U (1954) *Snow crystals* (Harvard University Press, Cambridge).
42. Bauser E & Strunk H (1981) Analysis of dislocations creating mono-molecular growth steps. *Journal of Crystal Growth* 51(2):362-366.
43. Frank FC (1981) Edge dislocations as crystal growth sources. *Journal of Crystal Growth* 51(2):367-368.
44. Malkin AJ, Kuznetsov YG, Glantz W, & McPherson A (1996) Atomic force microscopy studies of surface morphology and growth kinetics in thaumatin crystallization. *Journal of Physical Chemistry* 100(28):11736-11743.
45. Malkin AJ, Kuznetsov YG, & McPherson A (1999) In situ atomic force microscopy studies of surface morphology, growth kinetics, defect structure and dissolution in macromolecular crystallization. *Journal of Crystal Growth* 196(2-4):471-488.
46. Hobbs PV (1974) *Ice physics* (Clarendon Press, Oxford) pp 18-44.
47. Kuroda T & Lacmann R (1982) Growth kinetics of ice from the vapor phase and its growth forms. *Journal of Crystal Growth* 56(1):189-205.

Figure Legends

Fig. 1. Photomicrographs of the surface morphology on the basal face of a Ih ice crystal. The sequence of micrographs show the time course of a 2D nucleation growth of birth-and-spread type: 0 s (a), 0.57 s (b), 1.14 s (c) and 1.72 s (d). Cross marks in b and d show the regions at which contrast between the coalesced steps disappeared. Growth conditions: T_{sample}=-10.0 and T_{source}=-9.3°C. To obtain these images, raw images were processed according to the recipe explained in Fig. S1.

Fig. 2. Positions at which the 2D nucleations (asterisk marks in a) and the coalescences of adjacent 2D islands (cross marks in b) occurred, during 100s, on top of the basal face of the ice crystals shown in Fig. 1. Growth conditions: T_{sample}=-10.0 and T_{source}=-9.3°C. The asterisk and cross marks were placed on the time-averaged image shown in Fig. S1b.

Fig. 3. A schematic drawing of a cross section of a Ih ice crystal. Gray and red atoms correspond to oxygen and hydrogen, respectively. Bilayers made of water molecules are stacked in the *c* direction at 0.37 nm intervals.

Fig. 4. Photomicrographs of the surface morphology on the prism face of a Ih ice crystal. The sequence of micrographs show the time course of a 2D nucleation growth of birth-and-spread type: 0 s (a), 0.99 s (b), 1.98 s (c) and 2.97 s (d). Cross marks in b and d show the regions at which contrast between the coalesced steps disappeared. Growth conditions: T_{sample}=-2.2 and T_{source}=-2.2°C. To obtain these images, raw images were processed according to the recipe explained in Fig. S1.

Fig. 5. Photomicrographs of a basal face (a) and a prism face (b) of Ih ice crystals grown by the spiral growth mechanism induced by screw dislocations (indicated by white arrowheads). These two crystals were located adjacently on the same AgI crystal. As a result, it can be expected that the supersaturations provided for both crystal surfaces were almost the same. Growth conditions: T_{sample}=-15.0 and T_{source}=-16.0°C. Although T_{sample} was slightly higher than T_{source}, the growth of elementary spiral steps indicated that water vapor was still supersaturated. Details are explained in the Materials and Methods section. To obtain these images, the series of image processing used in Figs. 1 and 4 was not performed. Just the gain and offset of the original images were adjusted.

Fig. 6. Schematic drawings of the experimental setups: (a) the LCM-DIM system, the observation chamber and the water-vapor supply system; (b) a cross sectional view of the observation chamber; (c) and (d) ordinary bright-field optical microscopy images and crystallographic orientations of ice crystals nucleated heteroepitaxially (c) and randomly (d) on the cleaved AgI crystal at -15°C. In b, the upper right inset shows a closeup view of the cleaved AgI crystal attached to the upper Cu plate; the upper center inset presents a photomicrograph of the Ih ice crystals grown heteroepitaxially on the AgI crystal; the upper left inset depicts the morphology of the Ih ice crystal. The surface of the cleaved AgI crystal was observed from below through a triple window made of three glass plates of 150 μm thickness and rubber O-rings. In d, white arrowheads indicate prism faces, which are connected to the targeted prism face and are used to identify the crystallographic orientation.

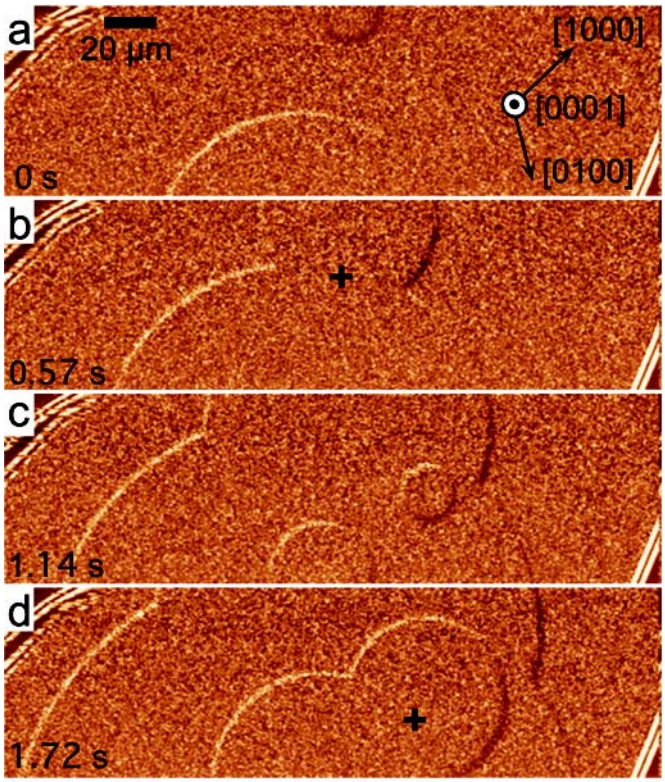

Fig. 1. Photomicrographs of the surface morphology on the basal face of a Ih ice crystal.

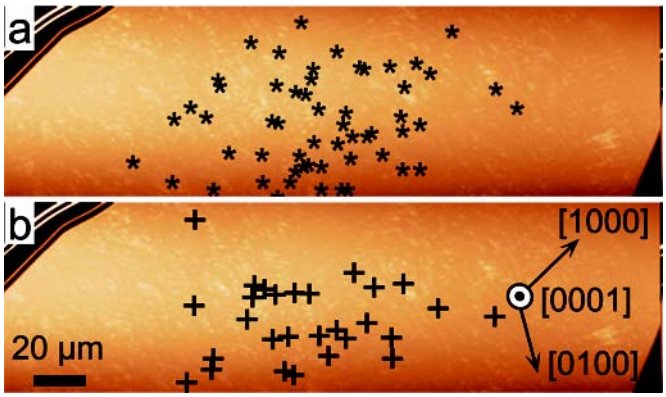

Fig. 2. Positions at which the 2D nucleations (asterisk marks in a) and the coalescences of adjacent 2D islands (cross marks in b) occurred, during 100s, on top of the basal face of the ice crystals shown in Fig. 1.

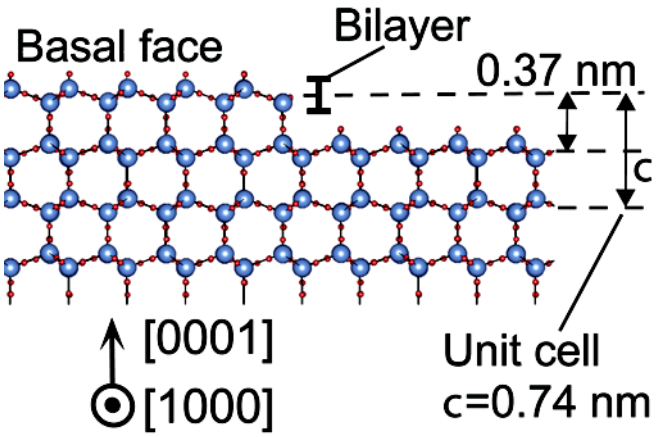

Fig. 3. A schematic drawing of a cross section of a Ih ice crystal.

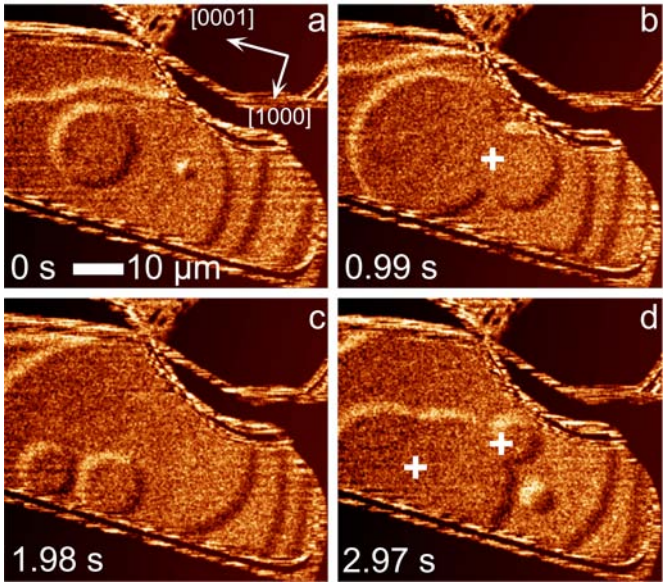

Fig. 4. Photomicrographs of the surface morphology on the prism face of a Ih ice crystal.

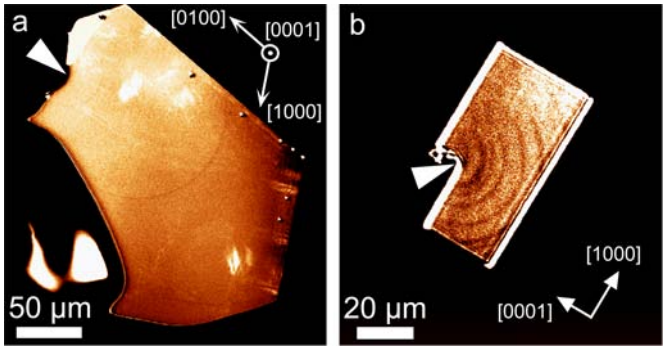

Fig. 5. Photomicrographs of a basal face (a) and a prism face (b) of Ih ice crystals grown by the spiral growth mechanism induced by screw dislocations (indicated by white arrowheads).

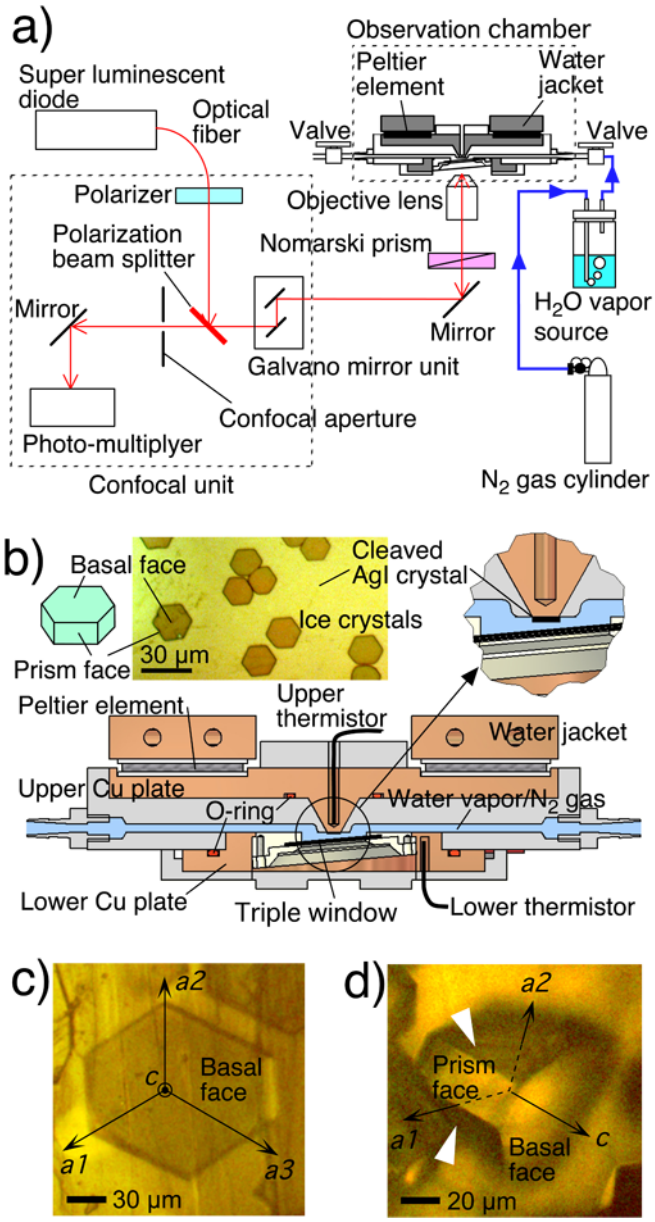

Fig. 6. Schematic drawings of the experimental setups: (a) the LCM-DIM system, the observation chamber and the water-vapor supply system; (b) a cross sectional view of the observation chamber; (c) and (d) ordinary bright-field optical microscopy images and crystallographic orientations of ice crystals nucleated heteroepitaxially (c) and randomly (d) on the cleaved AgI crystal at -15°C.

Supporting Information

Fig. S1. The image processing performed to obtain the images shown in Figs. 1 and 4. A time-averaged image (b) was subtracted from the original image (a). In b, motionless objects such as defects (a white arrowhead) and the inhomogeneous background level were extracted. After the gain and offset of the subtracted image was adjusted (c), a Gaussian filter of one pixel size was performed (d) to smooth the image. The images in Figs. S1d and 1d are identical.

Fig. S2. Photomicrographs of the basal face of the Ih ice crystal shown in Fig. 5a. In this figure, the ice crystal was grown by the same spiral growth mechanism (a white arrowhead shows the position of a screw dislocation) under higher supersaturation than that in Fig. 5a. Growth conditions: T_{sample}=-15.0 and T_{source}=-14.5°C. The distance between adjacent spiral steps shown in this figure is much smaller than that in Fig. 5a because of the higher supersaturation. As in the case of Fig. 5, to obtain these images, the series of image processing used in Figs. 1 and 4 was not performed. Just the gain and offset of the original images were adjusted.

Fig. S3. Micrographs of the cleaved surface of a gypsum crystal. The same crystal surface was observed by both LCM-DIM (a) and AFM (b). The inset of b shows the height profile along the bold line A-B. To obtain the image a, the series of image processing used in Figs. 1 and 4 was not performed. Just the gain and offset of the original image were adjusted. From the comparison between the images a and b, it can be concluded that the steps of 0.75 nm height on a gypsum crystal surface could be visualized with sufficient contrast by LCM-DIM.

Fig. S4. An exploded diagram of the observation chamber shown in Fig. 6. Four Peltier elements were used to control separately the temperatures of the upper and lower Cu plates.

Movie S1. Time course of the surface morphology on the basal face of a Ih ice crystal. Photomicrographs of 720×208 pixels were acquired over a 0.57 s scan time. The movie taken at 0.57 s time intervals clearly demonstrates that the basal face was growing by a 2D nucleation growth mode of birth-and-spread type. The series of images shown in Fig.

1 corresponds to the frames from 103.50 to 105.22 s in this movie. Growth conditions: T_{sample}=-10.0 and T_{source}=-9.3°C. To obtain this movie, just the gain and offset of raw images were adjusted. The image processing shown in Fig. S1 was not performed. The comparison between this movie and Fig. 1 indicates that the image processing (Fig. S1) gave no effect on the picture of 2D nucleation growth: the appearance of 2D islands by 2D nucleation and the subsequent lateral growth of 2D islands.

Movie S2. Effects of the image processing. The original images of Movie S1 were processed according to the recipe explained in the supporting information Fig. S1. In this movie, the appearance and subsequent lateral growth of 2D islands can be observed more clearly than in Movie S1.

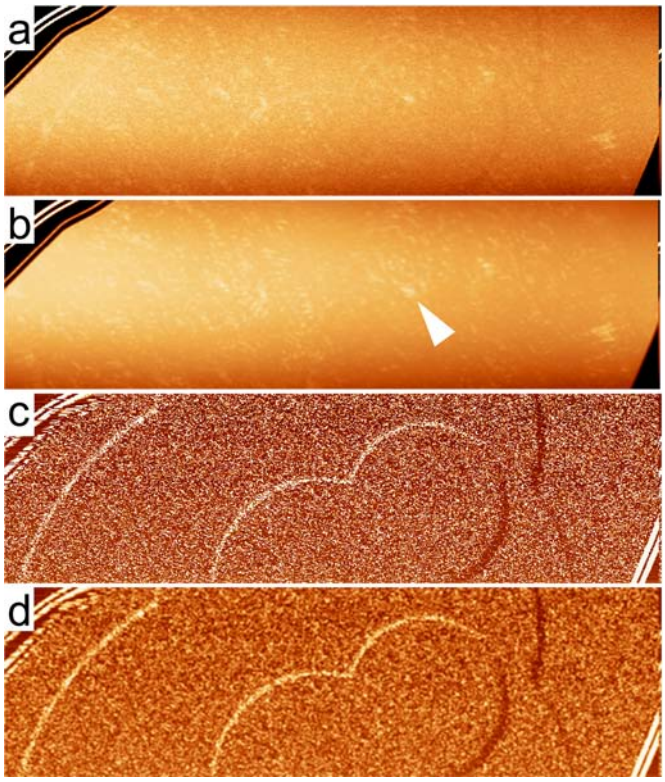

Fig. S1. The image processing performed to obtain the images shown in Figs. 1 and 4.

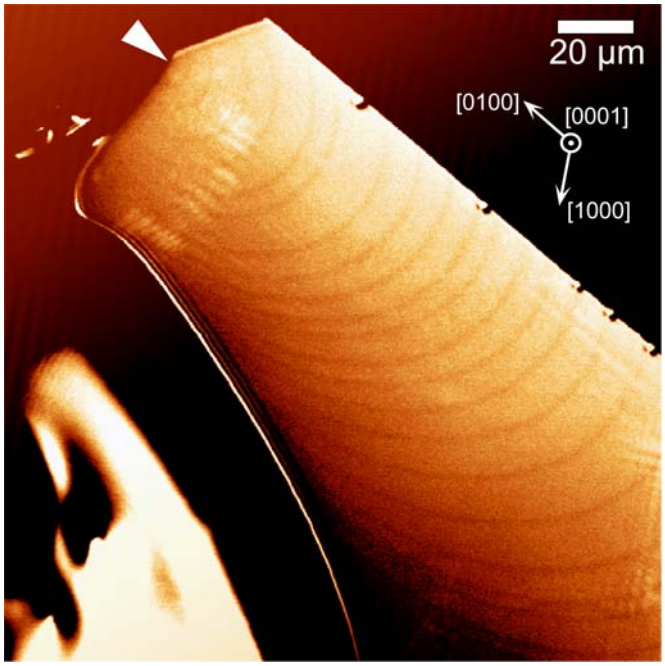

Fig. S2. Photomicrographs of the basal face of the Ih ice crystal shown in Fig. 5a.

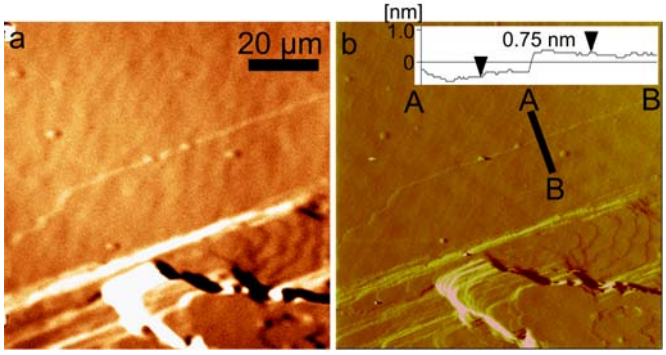

Fig. S3. Micrographs of the cleaved surface of a gypsum crystal.

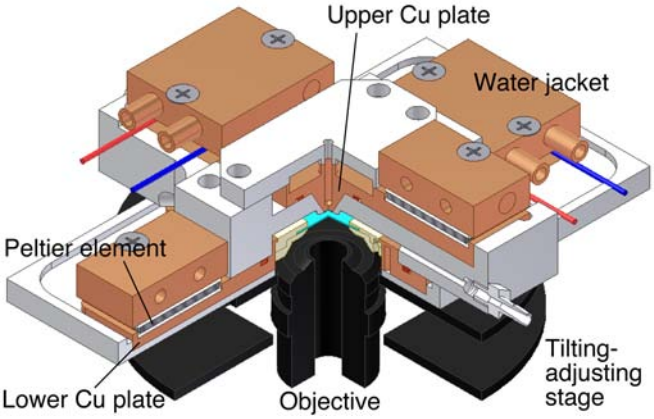

Fig. S4. An exploded diagram of the observation chamber shown in Fig. 6.

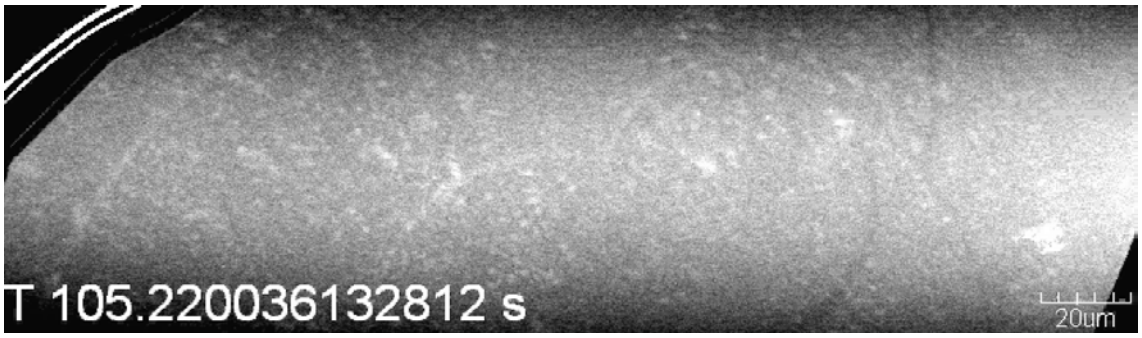

Movie S1. Time course of the surface morphology on the basal face of a Ih ice crystal.

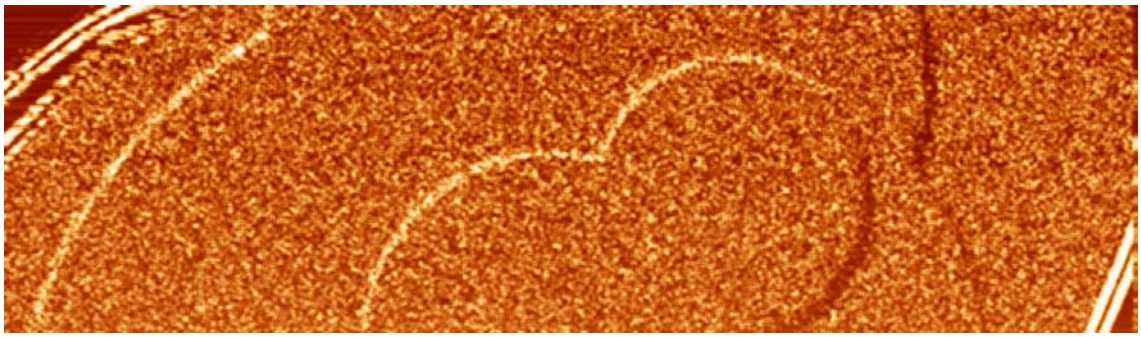

Movie S2. Effects of the image processing.